Chapter 5

Incorporation of cellulose in oxidative polymerization of PPy

5.1 Introduction

Cellulose is among the most abundant materials in nature derived from biomass with a structure of β-D-glucopyranose repeating units linked by (1-4)-glucosidic bonds and features with the features of low cost, high crystallinity and good mechanical properties [1]. Significant increase in research was devoted worldwide to application of cellulose; due to its increasing use in renewable, environmentally benign materials [2,3]. Application of cellulose includes uses in structural reinforcement of materials [4]. Cellulose is insoluble in water. However, its water solubility and infusibility can be improved by mixing organic acids such as dodecylbenzenesulfonic acid (DBSA), p-tolunesulfonic acid (PTSA) etc. as a dopant [5]. Cellulose based conducting polymer (CP) blends are typically flexible conductive materials which can be molded into different shapes [6]. Earlier investigations revealed that introduction of cellulose whiskers improved the mechanical properties of PPy, which has considerable intrinsic conductivity (10^{-4} to 10^{2} Scm^{-1}) at room temperature [7]. But processing is, however, troublesome because of its brittleness, poor compactability, poor heat annealing properties and very low solubility in most of the solvents [8]. Cellulose can be used in chemical polymerization of pyrrole for preparation of PPy-cellulose composite to overcome these problems, as it is a cheap and easily available bio degradable material. Recent advances shows that incorporation of Cellulose nanofibres (CNF) not only reinforced the brittle structure of PPy but also increased the surface area for PPy coating and enhanced the mechanical properties of cellulose [9]. Study of dielectric behaviour of such materials is important to know their electrical and optical properties for compatible potential applications.

Dielectric measurements were extensively used to study the energies of complex ionic defects also. Such studies on PPy based systems were reported by various workers, yet much more is still to explore. It is observed that the growth process of this type of materials is dependent on polymerization conditions such as time, temperature, pH of the medium etc. That is why it is thought worthwhile to have an in depth study on cellulose PPy composite. In this chapter, we report the effect of variation of polymerization time for cellulose-PPy composite to investigate dielectric and various other properties giving information about its morphology and structure. The composite is synthesized by means of chemical polymerization of pyrrole with cellulose in presence of DBSA, which acts as a dopant and also as a surfactant.

5.2 Experimental

300 mg cellulose powder is dispersed in 100 ml de-ionized water; 3 ml of Pyrrole (Py) is mixed with water to make 100ml by adding de-ionized water. The cellulose suspension added to the aqueous Py is placed in an ice bath and stirred constantly for 5 minutes. DBSA is added to the reaction mixture in molar ratio of 1:2 with pyrrole, and the mixture is kept under constant stirring for two hours in ice bath. Finally 8gm $FeCl_3$ is dissolved in 100 ml of de-ionized water and the solution is added to the suspension. The greenish black suspension is divided into three parts and subjected to magnetic stirring for three different polymerization times: for 6, 24 and 48 hours respectively. The reaction mixture is kept in an ice bath during the time of stirring. The resulting solution is filtered, washed with de-ionized water, and then dried in vacuum [10]. Three different samples so obtained for three different polymerization times, viz. 6, 24 and 48 hours are marked as sample A, B and C respectively. Films are cast on microscope slides (75 mm x 25 mm x 1.2 mm) from the reaction mixture and then oven dried at 60° C for 12 hrs. The thicknesses of the films are estimated by gravimetric method [11]. The composites are characterized for morphological, structural and dielectric properties

using SEM, TEM, FTIR, XRD and impedance analyzer. Impedance is measured at room temperature (30° C) in the frequency range 40Hz-40 KHz.

5.3 Results and Discussion

5.3.1 Scanning electron microscopy

SEM micrographs in Fig.5.1 shows the formation of nearly continuous matrix of cellulose with in-distinguished and irregular phase in the initial hours of polymerization but the particles gradually resumes regular morphology with increasing polymerization time and becomes spherical at 48 hours of polymerization time, as seen in their gradual changes in figures from 1A to C.

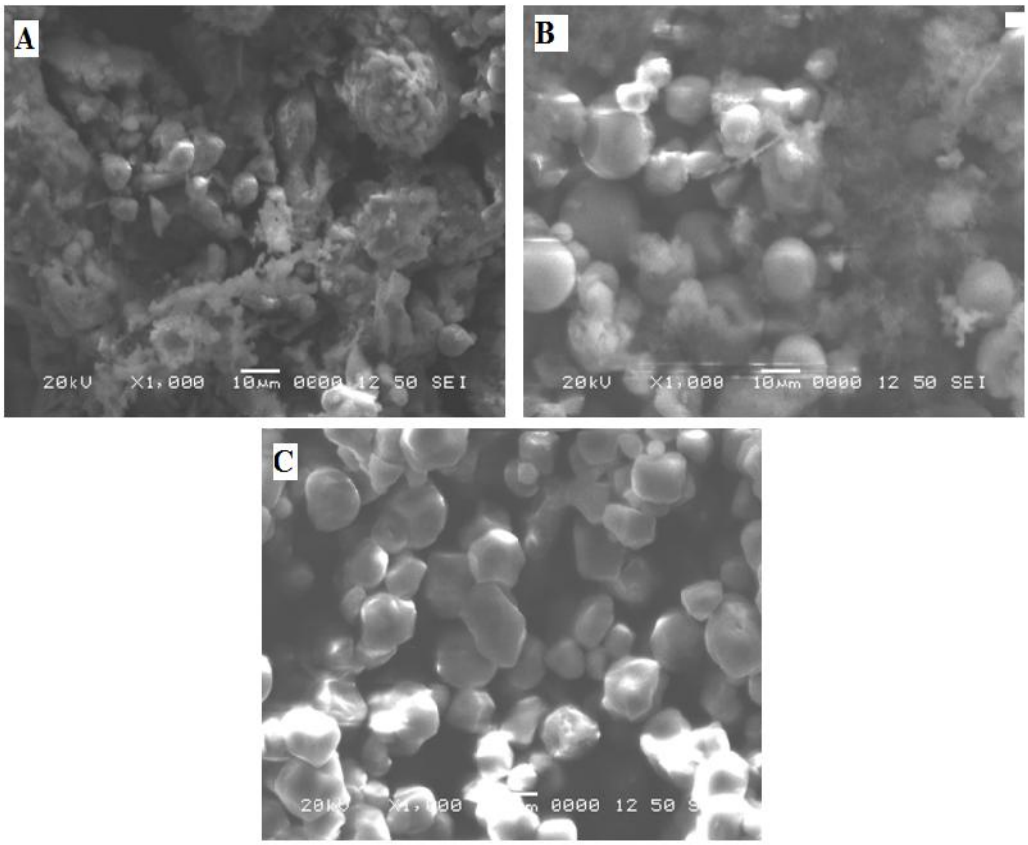

Fig.5. 1 SEM micrograph of the composite samples A, B and C (A for polymerization time t = 6 hours, B for t = 24 hours, C for t = 48 hours)

Such morphology was reported earlier for PPy-CNF composite [12]. It was reported that when CNF was introduced as additive in polymerization of pyrrole, PPy particles nucleated and grew up between the nanofibrils or over the surface of the residual fibers [13]. These PPy particles were reported to be of spherical shape and with size of the order of 100 nm [14]. We observe the particles with regular spherical shape after 48 hours of polymerization time. Adhesion of PPy particles over the cellulose surface is also observed which probably arises due to formation of H-bonds between cellulosic hydroxyl groups in presence of PPy. The spherical particles obtained by us are with average diameter of 16.9 in A, 18.9 in B and 19µm in C in their surface.

5.3.2 Transmission electron microscopy

TEM pictures shown in Fig. 5.2 depicts well dispersed cellulose polypyrrole composite in the initial hours of polymerization and increased polymerization time results in more compactness of the particles showing continuous matrix of cellulose around the PPy particles in irregular and

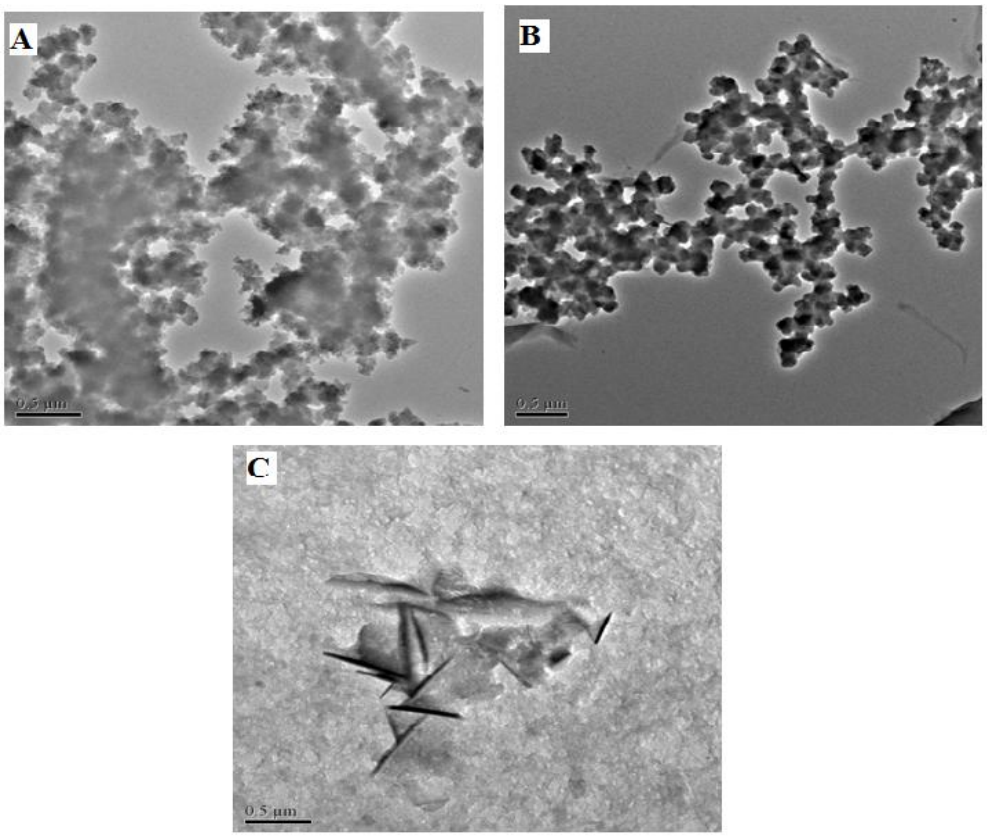

Fig. 5.2 TEM micrographs of the samples A, B and C (A for polymerization time t= 6 hours, B for t= 24 hours, C for t= 48 hours)

in-distinguished phase in the initial hours of polymerization which becomes more prominent with increased polymerization time. As shown in Fig. 2C, the particles become distinguished with a homogeneous layer of PPy formed over a fibrillar cellulosic matrix at this stage. Unlike the PPy particles in micro scale found in the surface, the TEM micrograph shows the formation of cellulose nanofibrils inside the surface which gradually formed a sheet with increasing polymerization time which is most prominent in sample C.

5.3.3 FT-IR spectroscopy

The FTIR spectra in Fig. 5.3 shows the peaks for cellulose at 3400 cm^{-1}, 2374 cm^{-1} and 1642 cm^{-1} with an arm associated at 1658 cm^{-1} in all the samples. Peak at 3404 cm^{-1} is due to

stretching of H-bonded ─ OH group [15] while at 1642 cm^{-1} is due to ─ OH group and C-chain vibration. Peaks due to cellulose molecule appear at 2374 cm^{-1} and 3400 cm^{-1} [16]. Characteristic pyrrole peaks are found in the range 1600 cm^{-1} to 700 cm^{-1} while the peaks formed at 1111 cm^{-1} and 1423 cm^{-1} are attributed to DBSA [17].

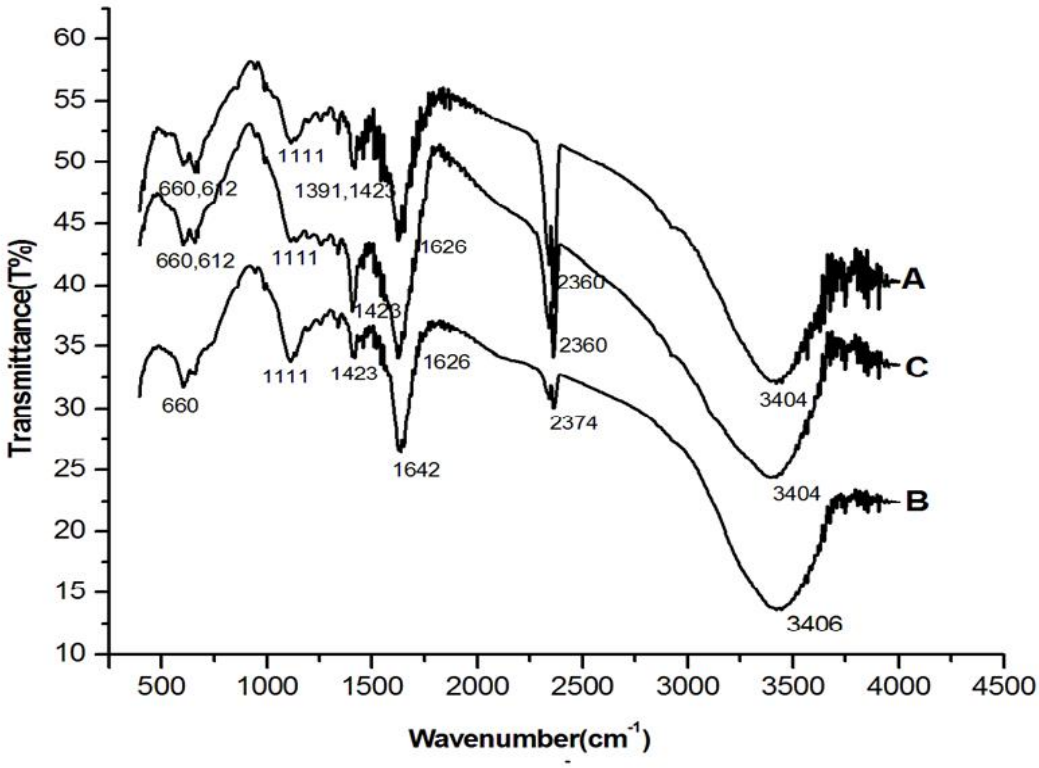

Fig.5.3 FT-IR spectra for A, B and C

(A for polymerization time t = 6 hours, B for t = 24 hours, C for t = 48 hours)

FTIR spectra reveal the formation of peaks characteristic of cellulose, pyrrole ring and doping anion vibration due to DBSA and confirmed the formation of PPy in presence of cellulose. Some peaks marginally shift with variation of polymerization time. Blue shift occurs for the characteristic vibration of main Pyrrole chain from 1626 cm^{-1} in A to 1642 cm^{-}

^{1} in C. This shift is due to modified stretching vibration of the main pyrrole ring. Such blue shifts are also observed in case of cellulose peaks of 3404 cm^{-1} and 2360 cm^{-1} in the spectrum of B and C. However, the peaks at 1111 cm^{-1} and 1423 cm^{-1} for DBSA remains unchanged indicating the fact that doping state with DBSA is unchanged with polymerization time. It is also observed that increase in polymerization time results in masking of certain peaks and matches with the results of SEM and TEM showing increased compactness and homogeneity of the particles with increased polymerization time.

5.3.4 X-Ray diffraction

XRD plots of the three samples are shown in Fig. 5.4. The peaks at 13.8° and 30.3° are for the composite with polymerization time of 6 hrs, while these positions are modified with change of polymerization time. Single peak is found at 26.6° for 24 hrs and at 26.2° for 48 hours.

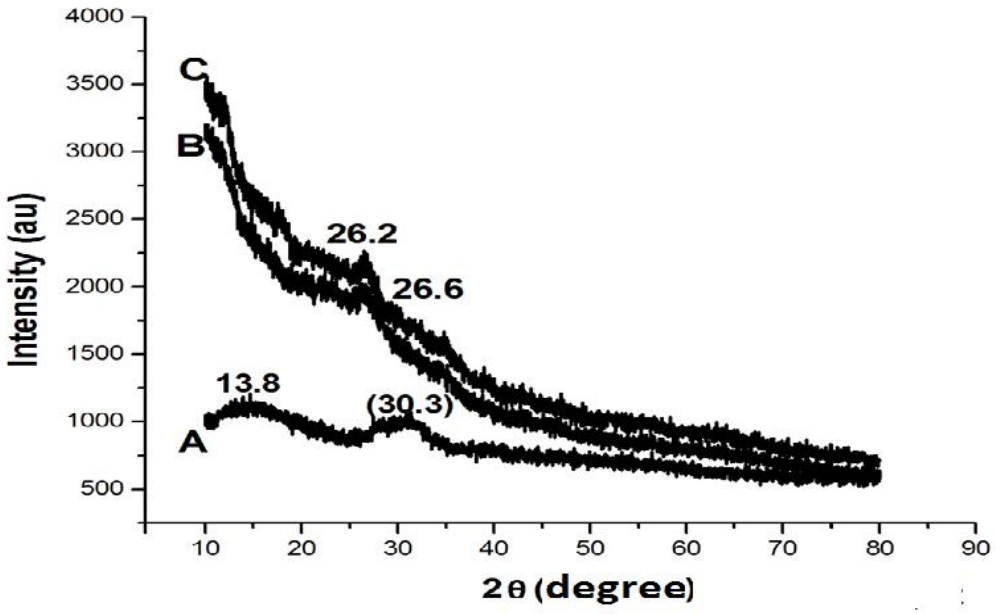

Fig. 5.4 XRD spectra for A, B and C (A for t = 6 hours, B for 24 hours, C for 48 hours)

The XRD pattern of the composite shows increase in peak intensity with decreasing value of scattering angle when the polymerization time is increased.

Though the formation of PPy reported earlier formed by chemical polymerization with $FeCl_3$ as oxidant showed amorphous nature [18], XRD profile of the composite presented here indicates increased homogeneity and crystallinity with increased polymerization time. The crystalline percentage in the three samples are measured by the relation [19],

$$X_c = \frac{A_c}{A_c + A_a} \times 100\% \text{ -------- (5.1)}$$

Where A_3 is the area of crystalline region and A_c is that of the amorphous region. The percentage of crystalline part is found to increase with polymerization time, from 40% in the sample A to 52% in B and 61% in C. To be shown later, conductivity and ionic mobility also increases, which agree with the results obtained from impedance analysis shown in the next sub-section. Thus the effect of increased polymerization time is to make the composite more homogeneous and isotropic with respect to ionic and electronic conduction.

5.3.5 Measurement of dielectric properties

The log-log plot for variation of dielectric constant ($\varepsilon^{/}$) vs frequency of the three samples are shown in Fig. 5.5, while Fig. 5.6 represents the plot of variation of dielectric loss ($\varepsilon^{//}$) vs frequency. $\varepsilon^{/}$ and $\varepsilon^{//}$exhibit stronger dispersion at low frequency range (40 Hz to 40 KHz) in good agreement with dielectric behavior of pure PPy reported earlier [20]. Dielectric response shows linear variation with strong low frequency dispersion for all the three samples. Such behavior probably arises due to strong tendency of the dipoles to orient themselves in the direction of the applied field [21]. The gradual exponential decrease in $\varepsilon^{/}$ with increasing frequency may be attributed to increase in charge carriers in the direction of

the field due to release of the frozen dipoles that consequently undergo co-operative movement with the adjoining segments in the main pyrrole chain [22]. The steady increase in charge carriers and their gradual reorientation in the direction of the applied field proceeds until saturation is reached when the dielectric loss becomes almost constant. Dielectric parameters as a function of frequency is calculated using the values of the equivalent parallel capacitance C_p, Dissipation factor D, and parallel equivalent resistance $R_{p,}$ in an RC circuit.

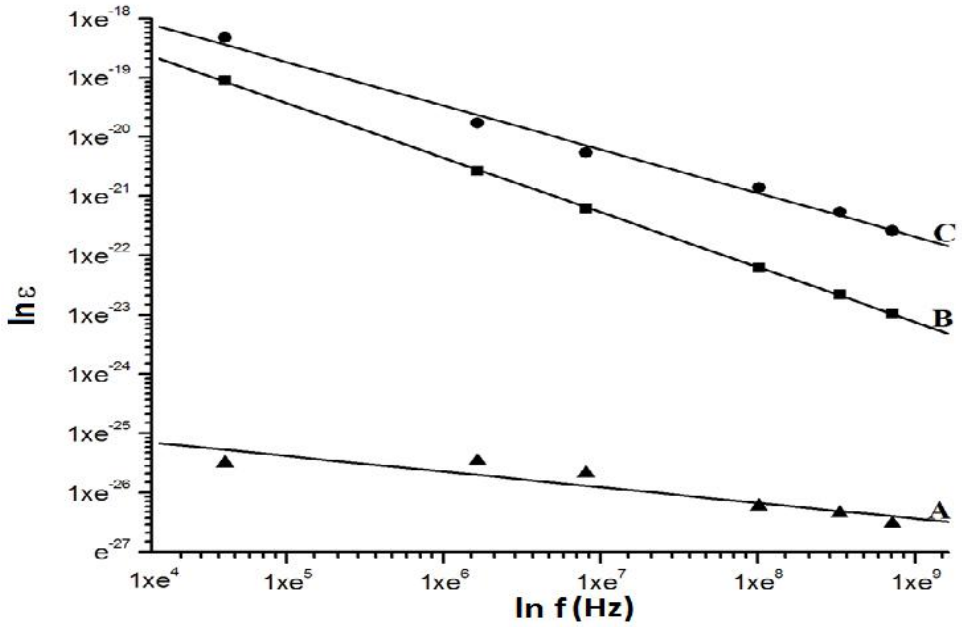

Fig. 5.5 Dielectric constant vs. frequency for A, B and C (A for t= 6 hours, B for 24 hours, C for 48 hours)

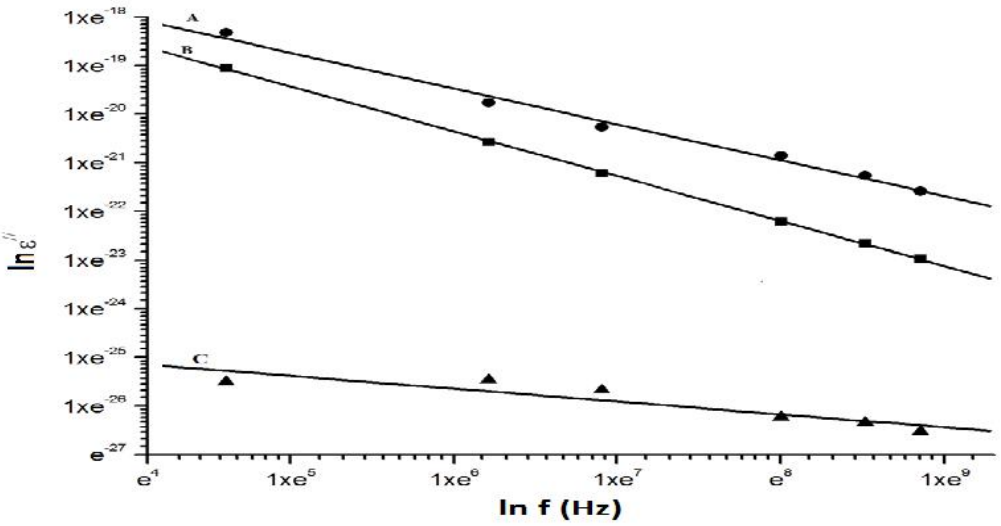

Fig. 5. 6 Dielectric loss vs. frequency for A, B and C (A for t = 6 hours, B for 24 hours, C for 48 hours)

The dielectric response of the composite samples may be described by a complex dielectric function as [23]

$$£'(f) = £'(f) + £''(f) \quad \ldots (5.2)$$

The first term $£'(f)$ in the above equation (the real part) describes the elastic "loss free" reaction of the material due to the external field and is given by equation (ii) below, while the second term (the imaginary part) $£''(f)$ is associated with the frequency dependent conductivity [σ (f)] and is given by equation (iii) as,

$$£' = \frac{C_p}{C_0} \quad \ldots\ldots\ldots\ldots\ldots\ldots (5.3)$$

$$£'' = \frac{£'}{\mu C_p R_p} \quad \ldots\ldots\ldots\ldots\ldots (5.4)$$

Where $C_0 = 0.08854\frac{A}{t}$ is the air capacitance and taken as the capacitance of vacuum, considering that the geometry of vacuum is of the same dimension as that of the sample. The impedance measurement is carried out with thin films of area A and thickness 't', C_p is the capacitance measured in pF, $\mu = 2®f$ is the angular frequency of the alternating field and $D \equiv \tan ¢$ is the dissipation factor, where δ is the phase angle.

Linear log-log plots in Figs. 5.5 and 5.6 indicate power law behavior of the dielectric response with frequency (i.e. $\propto f^n$). The numerical value of the exponent n for the three samples A, B and C are obtained as -5.71× 10^{-14}, - 4.78 × 10^{-14} and -2.66 × 10^{-14} respectively for $\varepsilon^{/}$ and as, - 6.7×10^{-16}, -3.34×10^{-13} and - 6.29×10^{-13} respectively for $\varepsilon^{//}$. Lower value of the exponent for curve A implies that the elastic behavior of the material is stable in sample A, i.e. for the composite in the initial hours of polymerization, while it shows more turbulent behavior with increased polymerization time. Such behavior was earlier reported in case of PPy composite for dielectric loss with temperature [24].

Higher value of slope indicates smaller value of dielectric constant. Such behaviour was experimentally observed for Bi_4 Ti_3 O_{12} glass [25]. The corresponding impedance function can be expressed as,

$$Z^* = \frac{R_p}{1+(i\mu ²)^{\sim}} \quad \text{……..... (5.5)}$$

$$\text{Where} \quad ² = \frac{1}{\mu_0} = R_p C_p \quad \text{..... (5.6)}$$

is the relaxation time and the exponent α is a characteristic determined by the distribution pattern of relaxation time with $0 \le \sim \le 1$. In complex systems, such as polymer and polymer composites, with strongly divergent dipole behavior, a functional distribution of the

relaxation time is observed when exposed to an external alternating field. The distribution pattern is a function of temperature also [26].

5.3.6 AC conductivity measurement

The log-log plot for conductivity vs. frequency is shown in Fig. 5.7. This again shows similar power law behavior. The frequency range in which this law applies is not exactly same in all the three samples. While the conductivity follows this power law up to 10 KHz from the starting frequency of 40 Hz in case of A and C, which is found to be valid up to 7 KHz in case of B. An explanation of this anomalous behavior by the sample B may be given on the basis of frequency dependent conductivity given by equation (5.7) [27],

$$\pm(\mu) = \pm_{dc}\left[1+\left(\frac{\mu}{\mu_h}\right)^s\right] \quad \ldots\ldots\ldots\ldots\ldots (5.7)$$

Where σ_{dc} is the dc conductivity, ω_h is the hopping frequency of the charge carriers and *s* is the exponent characterizing the nature of distribution lying in the range $0 \le s \le 1$ [28].

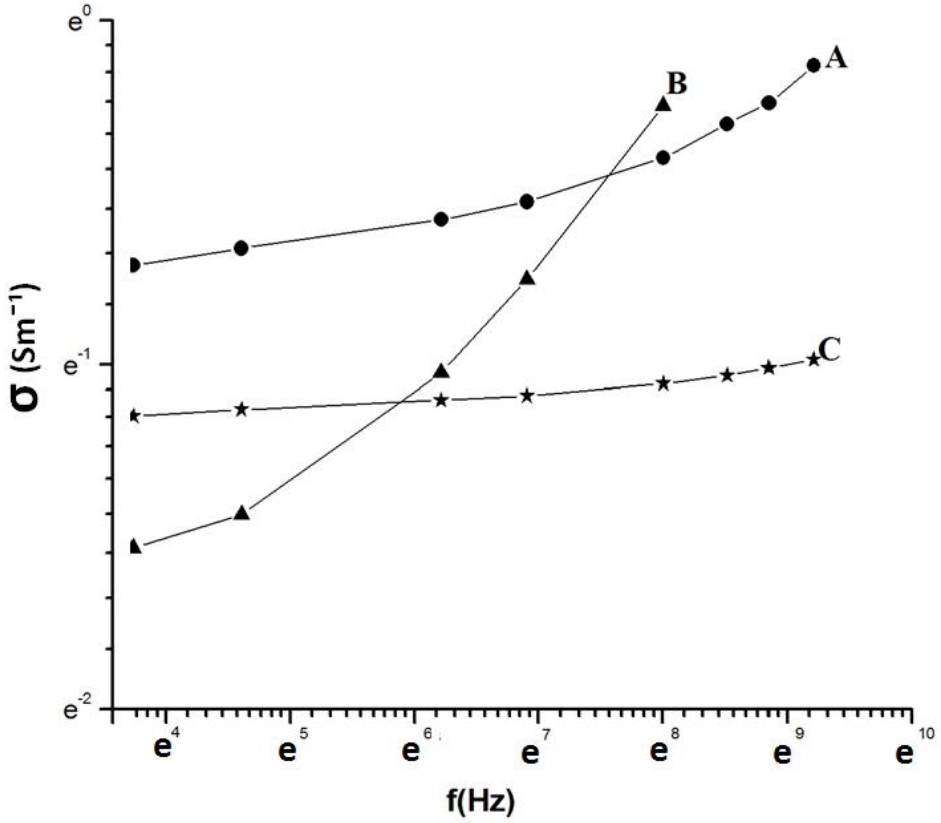

Fig. 5.7 Conductivity vs. Frequency for A, B and C (A for polymerization time t= 6 hours, B for t= 24 hours, C for t= 48 hours)

From extrapolation of Fig. 5.7, σ (ω) tends to σ_{dc} as ω approaches zero, which is observed in the plateau region of the three curves at low frequency. It is to be noted that there is gradual increase in conductivity with increase in frequency for samples A and B but in case of sample C, it is a flat straight line in the entire frequency range, indicating uniform value of conductivity over that range. This can be explained from the fact that frequency dependence of ac activation energy, which determines the relaxation time τ, figured in equation 5.5 above and responsible for release of frozen dipoles, is not very effective at room temperature range. Thus the hopping frequency in the low frequency range at a lower temperature is much higher. However, with increased frequency a threshold comes when further release of dipoles

is not permitted and a breakdown is encountered [29]. This happens for the sample B after 7 KHz. However, in case of sample C more number of frozen dipoles is released and the situation is similar to an environment of increased thermal energy. This results in decrease in hopping frequency so that dc activation energy and hence dc conductivity dominates over the small ac value, and conductivity σ (ω) remains almost constant in the entire range up to 10 KHz. This type of behavior commonly known as "universal dielectric response" or quasi dc (QDC) process is suggested to be a characteristic dielectric feature of PPy [30]. The changing trend of polarization forming a layer of space charges between the valence and conduction band ceases after the threshold frequency when saturation is reached and anomalous change in conductivity is observed [31,32].

5.4 Conclusion

Cellulose PPy composite is successfully prepared and characterized. TEM and XRD indicate formation of well dispersed PPy in cellulose matrix in the initial hours of polymerization and increased polymerization time results in more homogeneity and compactness of the particles. Spherical shaped particles are observed in SEM micrographs which are more prominent and distinguished with increase of polymerization time. Particle size as measured from TEM micrographs are found in nanometer range with cellulose nanofibrils (CNF) superposed over PPy nano particles. It may be suggested that modification of shape and size of the particles are attained by varying polymerization time and the micro molecular cellulose powder is converted into Nano Fibrillar Cellulose (NFC) in the PPy matrix at the maximum polymerization time used. Impedance analysis shows frequency dependent dielectric constant showing anomalous dispersion at low frequency range and becoming constant at high frequency. Dispersion in dielectric loss and dielectric constant arise possibly due to hopping

of polarons and bipolarons in the composite. This behavior is attributed to intra cluster charge carrier hopping arising out of interpenetration of PPy particles in cellulose structure.

5.5 References

1. R. Morent, N. De Geyter, J. Verschuren, K. De Clerck, P. Kiekens, and C. Leys, *Surf. Coat.Technol.* 202, 2008, 3427.

2. M.J Silva, A.O. Sanches, L.F. Malmonge, E.S. Madeiros, F.R. Morsyleide, C.M. Mcmahan, and J.M. Malmonge, *Macromol. Symp.* 319, 2012,196.

3. B. David, A. Sabrine, B.Sami, C. Didier and P. Nortier, *Cellulose* 13 ,2006,725.

4. B. Deepa, E. Abraham, B.M. Cherian, A. Bismarck, J.J. Blaker, L.A. Pothan, A.L. Leao, S.F. Souza and M. Kattaisami, *Bioresour. Technol.* 18, 2011, 443.

5. J.I. Moran, V.A. Alvarez, V.P. Cyras and A. Vazquez, *Cellulose* 15, 2008,149.

6. C. Sasso, *Macromol. Mater. Eng.* 295, 2010, 934.

7. G.F.S. Chen and H.Q. Liu, *J Appl Polym Sci.* 110, 2008, 641.

8. E. Jurgen and A. Kwasniewski, *Cellulose*, 9, 2002, 225.

9. A. Razaque. PhD Thesis. ACTA Universitatis Upsaliensis, Upsala, 2011.

10. X.S. Wang, H.P. Tang, X.D. Li and X. Hua, *Int J Mol Sci*, 10 ,2009, 5257.

11. A. Mihranyan, L. Neiholm, A.E. Garcia Bennett, and M. Stromme, *J Phys Chem B*, 112 ,2008, 12249

12. R.V. Stuart, *Vacuum Technology, Thin Films and Sputtering: An introduction*, Academic Press: New York, 2012.

13. J.H. Johnston, J. Moraes, F.M. Kelly, T. Borrmann, and D. Flynn, *Current Applied Physics*, 6 ,2006, 587.

14. X. Colom, F. Carillo, J.X. Sun, J.L. Ren, S. Curling, R.C. Sun, P. Fowler, and M.S. Baird, *Carbohydrate Research*, 341, 2006, 2677.

15. D. Fengel, *Holzforchung*, 47, 1993, 103.

16. S.Y. Oh, D.I. Yoo, Y. Shin, H.C. Kim, H.Y. Kim Y.S. Chung and W.H. Park, *Carbohydrate Research*, 340, 2005, 2376.

17. B. Hinterstoisser, M. Akerholm and L. Salmen, *Carbohydrate Research*, 334, 2001, 27.

18. D. Chunyue et al. *Cellulose*, 17, 2010, 106.

19. J. Bhadra, and D. Sarkar, *Ind. J. Phys.* 84 , 2010.

20. Y. Wang, Y. Fang, Z. Hu and Q. Wu, *Macromol Rapid Commun*, 27, 2006, 948.

21. V. Senthil, T. Badapande, Chithambararaj, A.C. Bose, A.K. Mohapatra, and S. Panigrahi, *J Polym Res*, 19, 2012, 9898.

22. R. Seoudi, A.B. El Beilly, W. Eisa, A. Shabake, S.I. Soliman, R.K. Abd Al Hamid, and R.A. Ramadan, *J. Appl. Sci. Res.* 8, 2012, 658.

23. J.H. Johnston, J. Moraes, F.M. Kelly, T Borrmann, D. Flynn, *Current Applied Physics*,6 ,2006, 587.

24. H. Yu, P. Chen, W. Chen and Y. Liu, *Cellulose*, 21, 2014, 1757.

25. C.H. Song, M. Kim, S.M. Lee, H.W. Choi, Y.S. Yang, *J Korean Phys Soc*, 56, 2010, 462.

26. P.S. Dutta, and S.K. De, *Material Research Bulletin*, 37, 2002, 139.

27. J.S. Kim, B.C. Choi, H.K. Yang and J.H. Jeong, *Journal of Korean Physical Society*, 52, 2008, 415.

28. N. Punaglek, A. Sittatrakul and W. Lerdwijitjarud, *Sci J. UBU*, 1 ,2010, 35.

29. H. Naceur, A. Megriche and M. El Maaoui, *Oriental Journal of Chemistry*, 29, 2013, 937.

30. S.A. Saafan, M.K. El-Nimr and E.H. ElGhazzawy, *J Appl Polym Sci*, 99, 2006, 3370.

31. A.K. Jonscher, *Universal Relaxation Law*, Chelsea Dielectric Press, London, 1996.

32. P.P.D. Sharma and D. Sarkar, *J Polym Maters*, 32, 2015, 497